

**Detecting the temporal structure of intermittent phase locking**

Sungwoo Ahn and Choongseok Park

*Department of Mathematical Sciences and Center for Mathematical Biosciences, Indiana University Purdue University, Indianapolis, Indiana 46202, USA*

Leonid L. Rubchinsky\*

*Department of Mathematical Sciences and Center for Mathematical Biosciences, Indiana University Purdue University, Indianapolis, Indiana 46202, USA and**Stark Neurosciences Research Institute, Indiana University School of Medicine, Indianapolis, Indiana 46032, USA*

(Received 14 March 2011; revised manuscript received 3 May 2011; published 5 July 2011)

This study explores a method to characterize the temporal structure of intermittent phase locking in oscillatory systems. When an oscillatory system is in a weakly synchronized regime away from a synchronization threshold, it spends most of the time in parts of its phase space away from the synchronization state. Therefore characteristics of dynamics near this state (such as its stability properties and Lyapunov exponents or distributions of the durations of synchronized episodes) do not describe the system's dynamics for most of the time. We consider an approach to characterize the system dynamics in this case by exploring the relationship between the phases on each cycle of oscillations. If some overall level of phase locking is present, one can quantify when and for how long phase locking is lost, and how the system returns back to the phase-locked state. We consider several examples to illustrate this approach: coupled skewed tent maps, the stability of which can be evaluated analytically; coupled Rössler and Lorenz oscillators, undergoing through different intermittency types on the way to phase synchronization; and a more complex example of coupled neurons. We show that the obtained measures can describe the differences in the dynamics and temporal structure of synchronization and desynchronization events for the systems with a similar overall level of phase locking and similar stability of the synchronized state.

DOI: [10.1103/PhysRevE.84.016201](https://doi.org/10.1103/PhysRevE.84.016201)

PACS number(s): 05.45.Xt, 05.45.Tp

**I. INTRODUCTION**

Synchronization of oscillations is a widespread phenomenon in physical sciences and beyond [1,2], including physiology [3] and neuroscience [4,5], and has been studied using approaches and methods of physics and nonlinear dynamics even in that applied context [6,7]. In particular, phase synchronization, dynamical phenomena where the phases of oscillations approach each other with time while both phases may remain chaotic and the amplitudes remain uncorrelated, appears to be quite common in nature and is well studied [1]. It is known that for some parameter values (usually, moderate coupling strength), phase synchronization can occur in an intermittent fashion [8–10]. It will present itself as an intermittent phase locking. The phase difference of two oscillators is close to constant during finite time intervals. These intervals of temporal synchronization epochs are random and interspersed by desynchronization events which are characterized by varying phase differences. Different types of intermittent behaviors may take place in different systems [10] and transition through intermittency may depend on the geometric structure of chaotic attractors [11]. Three types of intermittencies have been observed near the onset of phase synchronization: the type-I intermittency [8], the eyelet intermittency [8,12], and the ring intermittency [9].

Different approaches to synchronization analysis exist. One may approach the problem from the time-series analysis perspective, characterizing how much time series are correlated in some particular sense. This view essentially tells how close we

are to the synchronized state. Another approach is to study the stability of the synchronized state, via, for example, Lyapunov exponents, so that small positive Lyapunov exponents will describe the weak instability and, potentially, intermittency of synchronization. Lyapunov exponents, distribution of durations of synchronized episodes, and so on are ways to explore the synchronized state (synchronization manifold). Certain universality of behavior of a weakly unstable synchronization is expected and is captured by these approaches. Studies of Lyapunov exponents spectra [13] may go further and explore the dynamics of synchronous and desynchronous states in the vicinity of the saddle-node bifurcation point. However, these approaches become less powerful when the system is far away from the bifurcation point and do not describe the desynchronized episodes of intermittent or otherwise variable and weak synchronization in a large domain of parameter space. The desynchronized dynamics (“rejection mechanisms” in intermittency terminology) may be not universal and depend on the peculiarities of the system under study.

If the system is in an imperfectly synchronized state but is still close to the synchronization threshold (the case, which is probably expected in many physics or engineering applications), it spends most of the time in an almost synchronized state (near the synchronization manifold) and the focus on this state is natural. However, the synchrony can be weak. In particular, in living systems the synchronization may be very imperfect and weak, and too strong synchrony (high degree of temporal coordination) may be responsible for pathological states, such as schizophrenia or Parkinson's disease [14,15]. In terms of the phase space, the system spends a relatively small fraction of time near the synchronization manifold in the phase space. Thus even if Lyapunov exponents or distributions of the

\*leo@math.iupui.edu

durations of synchronized episodes may be informative about this part of dynamics, they do not tell much about dynamics overall because it is mostly desynchronized. This calls for the study of the highly variable synchrony and for the study of the structure of the phase space away from the relatively strongly unstable synchronization manifold. One may not expect much of universality here, but the characterization of this dynamics should be possible.

One approach is to characterize the degree of synchronization for a series of sliding time windows and obtain statistical estimates of significance (as in, for example, Ref. [16]). This may reveal important details of synchronized dynamics, not accessible otherwise (as in Ref. [17] for the case of tremor oscillations). However, synchronization is not instantaneous phenomena, so this approach is not designed to detect changes in the dynamics on the very short time scales. Yet, changes of this kind (very intermittent, variable synchronization) have been observed experimentally and have been conjectured to have functional significance [18,19].

Another example, where the fine temporal details of synchrony may be relevant may come from ecological dynamics. Synchronization in ecological dynamics is hardly perfect. It was conjectured that prolong zero-lag synchronization elevates the risks of extinction, so that there is an interest in these cases (reviewed in, e.g., Ref. [20]). One may want to distinguish between the moderate level of synchrony with few prolonged synchronized episodes and many short synchronized episodes.

Here we expand on the approach of Ref. [18] and study a method to analyze intermittent and weak phase locking from the nonlinear dynamics perspective. This approach is based on the constructions of the first-return maps for the difference of phases, partition of the resulting phase space into synchronized and nonsynchronized regions, and the analysis of the transitions between them. We show that for the case when some overall level of phase locking is present, one can characterize how this phase locking (properly defined) is gained, maintained, or lost for each cycle of oscillations and what it means in terms of the organization for the phase space of a coupled oscillators system. We do so with examples drawn from several typical model systems, ranging from simple coupled tent maps to more realistic conductance-based models of coupled cells. We also show how one can characterize the differences in the dynamics of coupled systems, which undergo through the same kind of intermittency and possess the same stability properties of synchronization manifold.

The structure of this paper is the following. Section II presents the set up of the method. Section III considers the method as applied to the dynamics of simple coupled maps. Section IV considers different types of intermittencies for phase synchronization. Section V illustrates the ideas of the paper for a more complex dynamical system. Finally, in Sec. VI we discuss the main ideas behind the method, summarize its properties, and discuss its applicability and possible further developments.

## II. METHODS TO STUDY THE TEMPORAL VARIABILITY OF THE SYNCHRONIZATION

Suppose that two oscillatory signals allow for a reasonably good reconstruction of their phases  $\phi_1(t)$  and  $\phi_2(t)$ . In a

discrete-time version (and thus applicable to experimentally obtained data) one can consider a standard index to characterize the strength of the phase locking between these two signals

$$\gamma = \left\| \frac{1}{N} \sum_{j=1}^N e^{i\theta(t_j)} \right\|^2, \quad (1)$$

where  $\theta(t_j) = \phi_1(t_j) - \phi_2(t_j)$  is the phase difference. This synchronization index varies from 0 to 1, that is, from a complete lack of phase locking to perfect phase locking (and does not tell anything about the amplitudes of the signals). One may also compute Lyapunov exponents, which characterize the stability of the synchronization manifold. In general, negative values of all transversal Lyapunov exponents are not necessarily sufficient to guarantee perfect synchronization [1], nevertheless their values describe the degree of stability or instability of the synchronized state and the strength of synchronization.

As we explained in the Introduction, these measures are not designed to describe the fine temporal structure of the dynamics, which motivates the following approach (its major steps were sketched by us in Ref. [18] and its explanation, validation, and properties are presented in subsequent sections of this paper). First, one needs to confirm that there exist some degree of phase locking between the phases of two variables  $x$  and  $y$ . This can be detected, for example, by computing Eq. (1) and comparing the resulting value of  $\gamma$  against some kind of significance value, computed analytically or via surrogates [16]. It should be emphasized here that our method allows for an analysis of the temporal development of phase difference if some level of synchrony (some preferred phase-locking angle) is present. It makes no sense if there were no synchrony between the signals at all.

Then set up a check point for the phase of  $y$ : whenever the phase of  $y$  crosses this check point from below, record the phase value of  $x$ , generating a set of consecutive phase values  $\{\phi_{x,i}\}$ ,  $i = 1, \dots, N$ , where  $N$  is the number of such level crossings in an episode under analysis. Then plot  $\phi_{x,i+1}$  versus  $\phi_{x,i}$  for  $i = 1, \dots, N - 1$ . The properties of these plots will characterize the dynamics of the synchronization. A tendency for predominantly synchronous dynamics will appear as a cluster of points, with the center at the diagonal  $\phi_{x,i+1} = \phi_{x,i}$ .

After determining the center of the cluster (that is, determining the preferred phase difference between two signals, at which they have the tendency to be locked) all values of the phases are shifted to a position with the center of the first region (quadrant) (see Fig. 1). This step is not necessary and is done here for the uniformity of the analysis. Then we consider how the system leaves the synchronization cluster and its vicinity and how it returns back to the synchronization by quantifying transitions between different regions of the  $(\phi_{x,i}, \phi_{x,i+1})$  space.

This phase space is then partitioned into four regions as illustrated in Fig. 1 [let us remind that the space of  $(\phi_{x,i}, \phi_{x,i+1})$  is, in fact, torus]. While the system is in the first region, it is considered to be in a synchronized state. Dynamics outside of the first region will be called a desynchronized state. Thus the synchronized state here is the one where the deviation

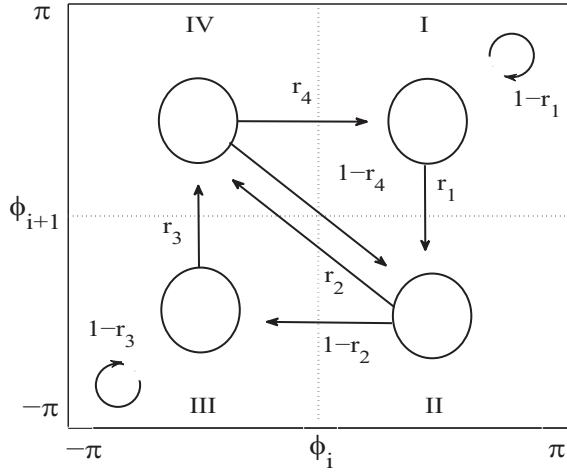


FIG. 1. Diagram of the  $(\phi_{x,i}, \phi_{x,i+1})$  first-return map. The arrows indicate all possible transitions from one region to another and the expressions next to the arrows indicate the rates for these transitions.

from the preferred phase angle is less than  $\pi/2$ . This is a compromise value: not too small to allow for some moderate fluctuations of the phases; not too large to allow for the phases to be sufficiently related and to be involved in some function. It also allows for symmetric partitioning of the phase space and definition of a few easy-to-compute transition rates (see below). Some situations may require a different definition of the synchronized state and the rest of the method will need to be modified. Nevertheless, even though this partition is quite coarse, it allows for an inspection of the fine temporal details, as we will show below. Four resulting regions in the phase space are numbered in a clockwise manner (Fig. 1) since this is the primary direction of the dynamics. An example of the first-return map for two coupled Lorenz oscillators is presented in Fig. 2 (a detailed study of this system with the method described here is in Sec. IV, see Fig. 7).

Transition rates  $r_i$  ( $i = 1, 2, 3, 4$ ) for the transitions between four regions of the map are defined as the number of points in a region, from which the system leaves the region, divided by the total number of points in that region. For example,  $r_1$  is the ratio of the number of trajectories escaping the first region for the second region to the number of all points in the first region. While the time-averaged measures of synchrony characterize whether the synchronization is strong or weak overall, utilization of these rates lets us explore the dynamics of the synchronization in time.

Further exploring the properties of the dynamics in the space  $(\phi_{x,i}, \phi_{x,i+1})$ , one may compute the relative frequencies of desynchronization events of different durations. In the considered first-return map approach, the duration of a desynchronization event is the number of steps that the system spends away from the first region minus 1 (because the point on the map has two coordinates, one of which is a “future” phase). The shortest duration of the desynchronization event corresponds to the shortest path 2-4-1 (note that the desynchronization will always start at the second region by virtue of our description of the dynamics). This will correspond to the desynchronization length of one cycle (in other words, in two cycles the phases are back in a locked state). If we

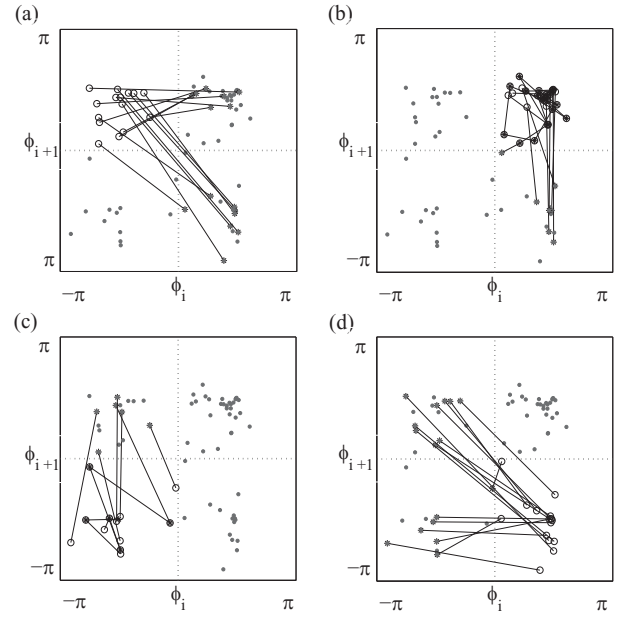


FIG. 2. An example of the first-return map for two coupled Lorenz oscillators. All four first-return plots have the same data points (gray circles), but each subplot (a–d) presents the evolution of points from one region (IV, I, III, and II, respectively). If a point evolves from one region to another region, then we represent it as  $\circ - *$ . If a point evolves within the same region, then we represent it as  $\circ - \circ$ . Thus each plot shows the transitions from a corresponding part of the phase space. We can compute the transition rates  $r_{1,2,3,4}$  from panels (b), (d), (c), and (a), respectively.

want to consider the chance of the duration of two cycles, we should consider the path 2-3-4-1. Longer desynchronization events will have many different paths corresponding to them. We will systematically compute the relative frequencies of the desynchronization events of different durations in Sec. IV for different systems.

The transition rates  $r_{2,3,4}$  are related to the durations of desynchronizations. Higher values of  $r_{2,3,4}$  promote short desynchronization episodes, while their low values promote long desynchronization events (note that for a well-synchronized dynamics, there may be very few points in the third quadrant, and numerical estimation of  $r_3$  may be unreliable). If transitions are independent then the relative frequencies of the durations of desynchronization events can be estimated by multiplying the corresponding rates of the transitions for different paths. For example, to estimate the probability of a desynchronization event of the shortest duration we should consider the shortest path 2-4-1 and the corresponding probability is  $r_2 r_4$ . This will correspond to the desynchronization length of one cycle. Longer desynchronizations will require summation of the products of rates corresponding to longer paths of equal length. In general, this independence (or near independence) may or may not be in place, but we consider several examples where the difference is not large and the rates  $r_{2,3,4}$  really describe the desynchronization durations.

The rate  $r_1$  is related to the averaged duration of the laminar phase and thus characterizes the property of the synchronized state. The average duration of the synchronized phase  $\langle \ell \rangle$

(for an intermittency near onset of phase synchronization, this quantity usually scales in a universal manner for specific intermittency types) is inversely proportional to  $r_1$

$$\langle \ell \rangle \sim 1/r_1, \quad (2)$$

and  $\langle \ell \rangle = 1/r_1$ , if  $\langle \ell \rangle$  is measured in the number of iterations of the map  $\phi_{x,i}$ , which is essentially the number of cycles of oscillations. The closer  $r_1$  is to 1, the more frequently the synchronized dynamics is interrupted.

Thus the rates permit evaluation of whether the weakness of synchrony is due to a few relatively long desynchronization events or a large number of short desynchronization events.

### III. COUPLED MAPS EXAMPLE

In this section we consider the behavior of rates for different parameter values (and thus for different transversal Lyapunov exponents of the synchronized state and the synchronization index  $\gamma$ ) in a simple system. We consider linearly coupled skew tent maps. This relatively simple map allows for the exact computation of Lyapunov exponents. The properties of the phase space depend on the parameters in a simple way. Thus we are able to see the relationship between the system's parameters, dynamics, Lyapunov exponents, and the rates  $r_i$ . This system is not necessarily an appropriate choice for the study of phase synchronization as a dynamical phenomenon when phases are correlated and amplitudes are not [21]. However we are not as much concerned with the phase synchronization per se in this sense, as we are concerned with a simple treatable example of the synchronous dynamics here. Therefore, coupled skew tent maps prove a possibility to illustrate our ideas in a simple system where analytical treatment is partially possible.

Consider a skew tent map

$$f(a,x) = \begin{cases} \frac{x}{a} & \text{if } 0 \leq x \leq a, \\ \frac{1-x}{1-a} & \text{if } a < x \leq 1, \end{cases} \quad (3)$$

where  $0 < a < 1$ . We will use two such maps with variables  $x$  and  $y$ . Let us consider the following coupling

$$\begin{aligned} x(t+1) &= (1-\varepsilon)f(a,x(t)) + \varepsilon f(a,y(t)), \\ y(t+1) &= \varepsilon f(a,x(t)) + (1-\varepsilon)f(a,y(t)), \end{aligned} \quad (4)$$

where  $\varepsilon$  is the coupling strength.

To characterize synchrony between  $x$  and  $y$ , we consider a new variable

$$\theta(t) = y(t) - x(t), \quad (5)$$

which will be an analog of the phase difference described above. In these coupled maps, synchronous state  $x = y$  is stable for  $\varepsilon > \varepsilon_c$  where the critical value  $\varepsilon_c < 1/2$ . Note that  $\theta$  in Eq. (5) varies between  $-1$  and  $1$  while the phase variable  $\phi_i$  in Fig. 1 varies between  $-\pi$  and  $\pi$ . In this section, we rescale the phase diagram accordingly to define the transition rates  $r_i$ .

Two Lyapunov exponents can be computed analytically (see, e.g., Ref. [1])

$$\begin{aligned} \lambda(a) &= -a \ln a - (1-a) \ln(1-a), \\ \lambda_{\perp}(a,\varepsilon) &= -a \ln a - (1-a) \ln(1-a) + \ln|1-2\varepsilon|. \end{aligned} \quad (6)$$

The first Lyapunov exponent  $\lambda(a)$  corresponds to the motion governed by the one-dimensional dynamical system  $x(t+1) = f(a,x(t))$  whose subspace is  $\{(x,y)|x=y\}$ . The second, transversal Lyapunov exponent  $\lambda_{\perp}(a,\varepsilon)$  characterizes the dynamics transverse to that invariant subspace. Note that  $\lambda(a)$  is always positive for  $0 < a < 1$  and has a maximum  $\ln 2$  at  $a = 1/2$ . Since  $\lambda_{\perp}(a,\varepsilon) = \lambda(a) + \ln|1-2\varepsilon|$ , the transversal Lyapunov exponent  $\lambda_{\perp}(a,\varepsilon)$  can change from positive to negative depending on  $a$  and  $\varepsilon$ . Both Lyapunov exponents are symmetric around  $a = 1/2$ . That is,  $\lambda(a) = \lambda(1-a)$  and  $\lambda_{\perp}(a,\varepsilon) = \lambda_{\perp}(1-a,\varepsilon)$ . The synchronization stability threshold  $\lambda_{\perp}(a,\varepsilon_c) = 0$  is reached at  $\varepsilon_c = \frac{1}{2} - \frac{1}{2}a^a(1-a)^{(1-a)}$ .

It is interesting to note that the coupled maps [Eqs. (3) and (4)] have exact solutions when the system is at a bifurcation point and is not robust. For example, for  $a = 1/2$  and  $\varepsilon = 1/4$  (and thus  $\lambda = \ln 2$  and  $\lambda_{\perp} = 0$ ) initial conditions  $(x,y) = (0.46,0.5)$  lead to a period-20 trajectory and initial conditions  $(x,y) = (0.044,0.052)$  lead to a period-100 trajectory. These trajectories are not hard to compute, and then one can formally compute  $r_i$  ( $r_1 = 2/5$ ,  $r_2 = 3/5$ ,  $r_3 = 2/5$ , and  $r_4 = 2/5$  for the former trajectory and  $r_1 = 13/25$ ,  $r_2 = 12/25$ ,  $r_3 = 13/25$ , and  $r_4 = 13/25$  for the latter). However, the system does not exhibit synchronous behavior, there is no single preferred value for the difference of variables  $\theta$ , and the computation of rates is not appropriate.

We numerically iterate the coupled maps [Eqs. (3) and (4)] and compute the rates  $r_i$  for different  $a$  and  $\varepsilon$ . We vary  $a$  from 0.125 to 0.35 with step size 0.025 and  $\varepsilon = [1 - ka^a(1-a)^{1-a}]/2$  where  $k$  varies from 1.05 to 1.45 with step size 0.05 (with this setup  $\lambda_{\perp} = \ln k$ ). Figure 3

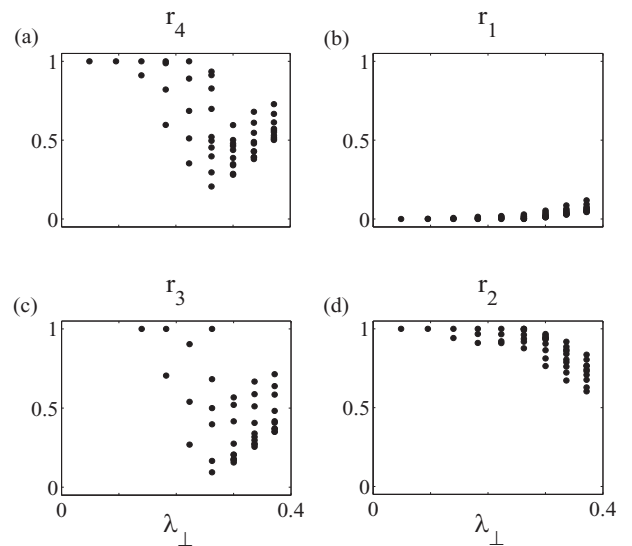


FIG. 3. We varied parameters  $a$  and  $\varepsilon$  to compute the transversal Lyapunov exponent  $\lambda_{\perp}$  and rates  $r_i$ . The rate  $r_1$  ( $r_2$ ) and  $\lambda_{\perp}$  have a positive (negative) relation. Rates  $r_3$  and  $r_4$  present more spread and more complex relationship with  $\lambda_{\perp}$ .

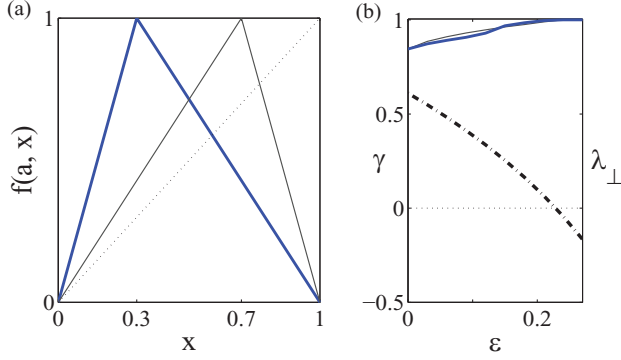


FIG. 4. (Color online) (a) Two skew tent maps for  $a = 0.3$  (thick solid line) and  $a = 0.7$  (thin solid line), respectively. (b) Transversal Lyapunov exponent  $\lambda_{\perp}$  (dash-dotted line) and two synchronization indices  $\gamma$  (thick solid line for  $a = 0.3$  and thin solid line for  $a = 0.7$ ). Two  $\gamma$  values are almost the same. Transversal Lyapunov exponent  $\lambda_{\perp}$  decreases as  $\varepsilon$  increases and crosses 0, when  $\gamma$  approaches 1.

shows the relationship between  $\lambda_{\perp}$  and the rates  $r_i$ . Each dot represents a different pair of  $(a, \varepsilon)$ . Since  $\lambda_{\perp}$  characterizes the evolution of the trajectory transverse to the invariant subspace  $\{(x, y) | x = y\}$ , the smaller  $\lambda_{\perp}$  corresponds to a less unstable manifold and more synchronized dynamics, which results in the smaller  $r_1$ . As  $\lambda_{\perp}$  decreases, the points  $(x, y)$  coalesce to the diagonal line  $x = y$  in the  $(x, y)$  plane. This shortens the duration of desynchronization events and increases the reinjection probability to the synchronous state. Thus,  $r_1$  tends to decrease while  $r_{2,4}$  tends to increase as  $\lambda_{\perp}$  decreases. However, one can clearly see that the same value of  $\lambda_{\perp}$  may correspond to drastically different rates and thus to different timing of synchronized and desynchronized dynamics.

If there is no point in the given region, then the transition rate at that region is undefined. As  $\lambda_{\perp}$  decreases, the system spends less and less time in desynchronous regions. This makes the number of points in the third region extremely small (or sometimes zero). Thus numerically computed values of  $r_3$  are less reliable in this case [or are undefined, as is the case of  $r_3$  for small  $\lambda_{\perp}$  in Fig. 3(c)].

We now consider some specific parameter values to show that the transition rates can effectively discriminate two different systems with identical  $\lambda_{\perp}$  and similar  $\gamma$ . Figure 4(a) shows coupled skew tent maps for  $a = 0.3$  and  $a = 0.7$ . Their two Lyapunov exponents are exactly the same because of their symmetry around  $a = 1/2$ , but the maps are different and their dynamics are different. Figure 4(b) illustrates how coinciding transversal Lyapunov exponents  $\lambda_{\perp}$  (stability property) and synchronization indices  $\gamma$  (average strength of phase locking) for both maps depend on  $\varepsilon$ . For these values of  $a$  the threshold value of coupling is  $\varepsilon_c \approx 0.2286$ .

However, Fig. 5 shows that the rates  $r_i$  for  $a = 0.3$  and  $a = 0.7$  are different and sometimes substantially different for a range of  $\varepsilon \in (0, 0.15)$ . The values of the rate  $r_1$  are essentially the same, as one may expect, because  $r_1$  is related to the stability of the synchronized state, which is the same for both cases. The other rates present a different picture. The system with  $a = 0.7$  (thin solid line in Fig. 5) has higher  $r_{2,3,4}$  for almost all ranges of  $\varepsilon$  than those of  $a = 0.3$  (thick

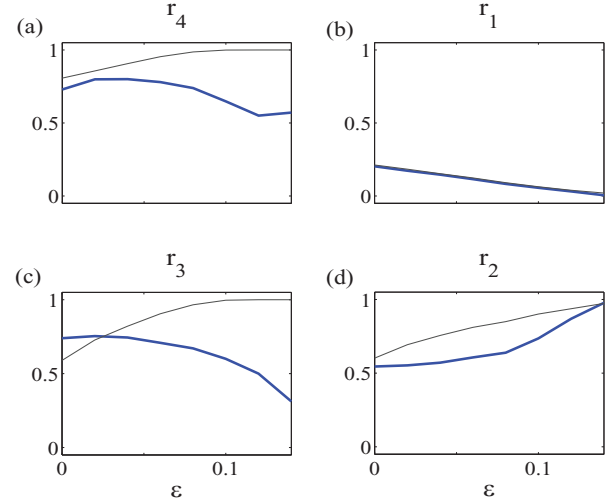


FIG. 5. (Color online) Transition rates for the linearly coupled skew tent maps for  $a = 0.3$  (thick solid line) and  $a = 0.7$  (thin solid line). We used 350 000 iterations and removed the first 50 000 iterations. Differences in the rates  $r_{2,3,4}$  are clearly visible.

solid line), which suggests the stronger tendency for shorter desynchronization events.

As the coupling  $\varepsilon$  increases to synchronization threshold value, the rates  $r_{2,3,4}$  are undefined while  $r_1$  decreases to zero. This is expected because the system spends most of (if not all) the time in the vicinity of the synchronized manifold. Thus, the dynamics is mostly synchronized and the rates are not very relevant. The rate  $r_1 \approx 0$  at  $\varepsilon \approx 0.15 < \varepsilon_c \approx 0.2286$ . This probably happens because our partition of the phase space of the first-return map for the phase difference implies that  $r_1 = 0$  and dynamics is synchronous when the deviation from the complete synchrony  $\theta = 0$  is less than  $1/2$ . But  $\theta(t)$  can still fluctuate in some smaller limits, which is what happens for  $\varepsilon$  in the interval of about  $(0.15, 0.2286)$ .

This simple case illustrates that although the stability of the synchronization manifold is the same for two systems, their dynamics can be substantially different. Lyapunov exponents and synchronization index  $\gamma$  naturally are unable to capture the differences. However, the analysis using the transition rates can distinguish two different systems and provide the temporal details of dynamical behaviors.

#### IV. ANALYSIS OF THREE DIFFERENT INTERMITTENCY TYPES

Intermittently synchronized dynamics can be observed near the boundary of synchronization. So far, three types of intermittencies near the onset of phase synchronization have been observed: the type-I intermittency [8], the eyelet intermittency [8,12], and the ring intermittency [9].

In this section, we will study these three types of intermittent behaviors in coupled chaotic oscillators with the techniques described in Sec. II. First, we will look at the type-I and the eyelet intermittencies in bidirectionally coupled Rössler oscillators and bidirectionally coupled Lorenz oscillators and then we will look at the eyelet and the ring intermittencies in unidirectionally coupled Rössler oscillators.

Intermittency types are characterized by the probability distribution of the laminar (synchronized in our context) phase length  $\ell$  and the scaling behavior of the mean laminar phase length  $\langle \ell \rangle$ . As far as the type-I and the eyelet intermittencies are concerned, coupled Rössler oscillators and coupled Lorenz oscillators with small frequency detuning show the same scaling properties of synchronous episodes near and away from the point of bifurcation [8,12]. However, we will show that there are important differences in the timing of dynamical behavior.

We consider two coupled chaotic Rössler oscillators

$$\begin{aligned} x'_{1,2} &= -\omega_{1,2}y_{1,2} - z_{1,2} + \varepsilon_{1,2}(x_{2,1} - x_{1,2}), \\ y'_{1,2} &= \omega_{1,2}x_{1,2} + 0.15y_{1,2}, \\ z'_{1,2} &= 0.2 + z_{1,2}(x_{1,2} - 10), \end{aligned} \quad (7)$$

where  $\omega_{1,2}$  are the natural frequencies of each chaotic oscillator and  $\varepsilon_{1,2}$  measure the strengths of the linear coupling. The phase difference is obtained by

$$\theta = \phi_1 - \phi_2 = \arctan\left(\frac{y_1}{x_1}\right) - \arctan\left(\frac{y_2}{x_2}\right). \quad (8)$$

We also consider two coupled chaotic Lorenz oscillators

$$\begin{aligned} x'_{1,2} &= 10.0(y_{1,2} - x_{1,2}) + \varepsilon(x_{2,1} - x_{1,2}), \\ y'_{1,2} &= (36.5 + \gamma_{1,2})x_{1,2} - y_{1,2} - x_{1,2}z_{1,2}, \\ z'_{1,2} &= -3.0z_{1,2} + x_{1,2}y_{1,2}, \end{aligned} \quad (9)$$

where  $\gamma_{1,2}$  are parameters for the frequency detuning of each chaotic oscillator and  $\varepsilon$  measures the strength of the linear coupling. As in Ref. [8], by defining a new variable  $u = \sqrt{x^2 + y^2}$  a phase can be defined on the  $(u, z)$  plane. The phase difference is obtained by

$$\begin{aligned} \theta &= \phi_1 - \phi_2 \\ &= \arctan\left(\frac{z_1 - \hat{z}_1}{u_1 - \hat{u}_1}\right) - \arctan\left(\frac{z_2 - \hat{z}_2}{u_2 - \hat{u}_2}\right), \end{aligned} \quad (10)$$

where  $(\hat{u}_1, \hat{z}_1), (\hat{u}_2, \hat{z}_2)$  are unstable fixed points in the middle of the trajectories rotating in the  $(u, z)$  plane.

### A. Type-I intermittency

In coupled Rössler oscillators, let us assume that the difference between  $\omega_1$  and  $\omega_2$  is small and the systems are bidirectionally coupled with  $\varepsilon_{1,2} = \varepsilon$ . When  $\omega_1 = 1.015$  and  $\omega_2 = 0.985$ , Lee *et al.* [8] found the first critical value  $\varepsilon_t = 0.0276$  where  $\theta$  increases in a nearly periodic sequence of  $2\pi$  jumps. They showed that for  $\varepsilon < \varepsilon_t$ , the mean laminar phase length  $\langle \ell \rangle$  obeys the scaling rule

$$\langle \ell \rangle \sim (\varepsilon_t - \varepsilon)^{-1/2}. \quad (11)$$

In coupled Lorenz oscillators, let us again assume that the difference between  $\gamma_1$  and  $\gamma_2$  is small. When  $\gamma_1 = 1.5$  and  $\gamma_2 = -1.5$ , Lee *et al.* [8] also found the first critical value  $\varepsilon_t = 6.7$ . The phase desynchronization occurs with  $2\pi$  phase slip, but it shows  $\pm 2\pi$  irregular phase jumping behaviors, which are different from coupled Rössler oscillators. However, the probability distribution of the laminar phase length  $\ell$  and the scaling rule of the mean laminar phase length  $\langle \ell \rangle$

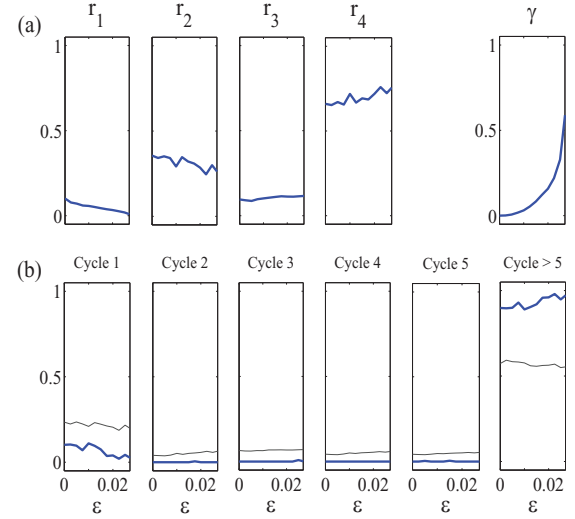


FIG. 6. (Color online) Synchronized dynamics of bidirectionally coupled Rössler oscillators in dependence on the coupling strength  $\varepsilon$ . Two critical values for intermittencies are  $\varepsilon_t = 0.0276$  and  $\varepsilon_c = 0.0286$ . (a) Rates  $r_i$  and synchronization index  $\gamma$ . (b) Relative frequencies of the desynchronization events of different durations (durations are measured in cycles of oscillations, i.e., in the number of iterations of the  $\phi_{x,i}$  map, see Sec. II). Thick solid line represents the actual relative frequencies of the desynchronization events of different durations, while thin solid line represents the relative frequencies, which would be there under the assumption of independent transition rates. The longer cycles of desynchronization are dominant relative to short cycles.

are the same as coupled Rössler oscillators. The scaling rule together with the corresponding probability distributions of synchronous episodes suggest that these two systems are in the type-I intermittency.

Figures 6 and 7 show the rates  $r_i$  and the relative frequencies of the desynchronization events of different durations for a range of coupling strength. By comparing Fig. 6 with Fig. 7, one can tell that two coupled systems exhibit different temporal features of the dynamics.

In Fig. 6(b), the probability of the long desynchronization events (longer than five cycles of oscillations) is in the range of about (0.8,0.9) while in Fig. 7(b), this probability is in the range of about (0,0.25). This is true, in particular, for similar values of  $\gamma$ . Since coupled Rössler oscillators have a high probability of long cycles, two oscillators spend a long time in the desynchronized state once the trajectory leaves the synchronous state. However, it does so very rarely. Coupled Lorenz oscillators (Fig. 7) present a different temporal dynamics. Short desynchronization cycles prevail and the comparable values of  $\gamma$  are reached with a larger number of short desynchronized episodes.

The relative frequencies of desynchronization events of different durations can be close to the relative frequencies estimates from the transition rates like Figs. 7(b) and 8(b) or can be different from these estimates like Figs. 6(b) and 9(b). The transitions between regions are not necessarily independent (or near independent). However, the estimated relative frequencies of desynchronization events of different durations still show some similar tendencies.

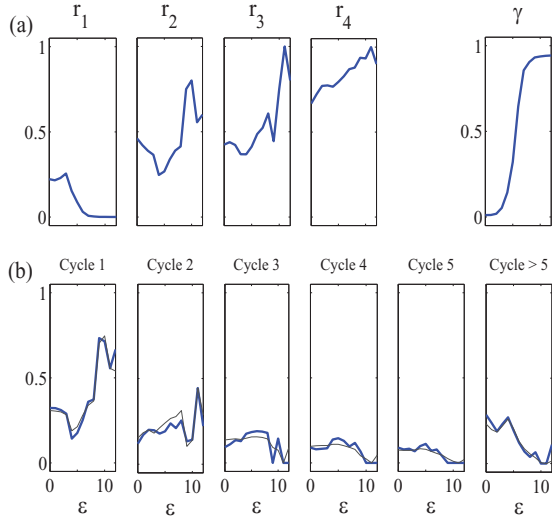


FIG. 7. (Color online) Synchronized dynamics of bidirectionally coupled Lorenz oscillators in dependence on the coupling strength  $\varepsilon$ . Two critical values for intermittencies are  $\varepsilon_t = 6.7$  and  $\varepsilon_c = 12$ . (a) Rates  $r_i$  and synchronization index  $\gamma$ . The behaviors of the rates and the durations of desynchronization events are different from coupled Rössler oscillators. (b) Relative frequencies of the desynchronization events of different durations (durations are measured in cycles of oscillations, i.e., in the number of iterations of the  $\phi_{x,i}$  map, see Sec. II). The thick solid line represents the actual relative frequencies of the desynchronization events of different durations, while the thin solid line represents the relative frequencies, which would be there under the assumption of independent transitions. Unlike Fig. 6, short desynchronization events dominate the dynamics.

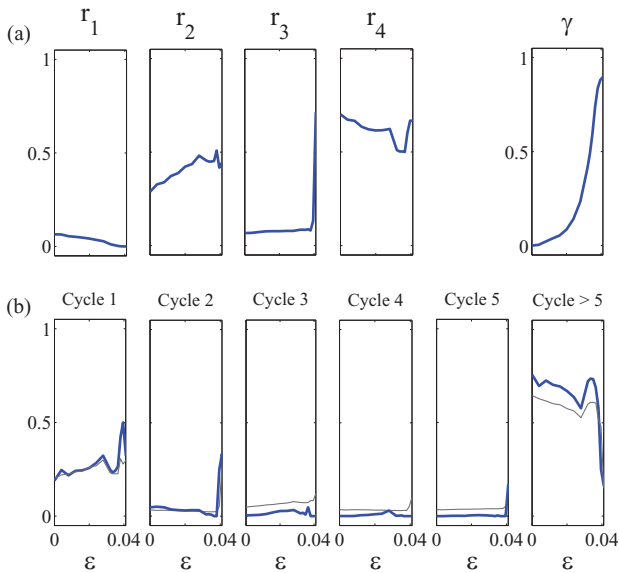


FIG. 8. (Color online) Eyelet intermittency in unidirectionally coupled Rössler oscillators with parameters  $\varepsilon_1 = 0$ ,  $\varepsilon_2 = \varepsilon$ , and control parameters  $\omega_1 = 0.93$ ,  $\omega_2 = 0.95$ . Two critical points are  $\varepsilon_t = 0.0345$  and  $\varepsilon_c = 0.042$ . (a) Rates  $r_i$  and synchronization index  $\gamma$ . (b) Relative frequencies of desynchronization events of different durations. The thick solid line stands for actual duration, while the thin solid line represents the estimates from the transition rates. The intermittent behavior is different from the bidirectionally coupled Rössler oscillators.

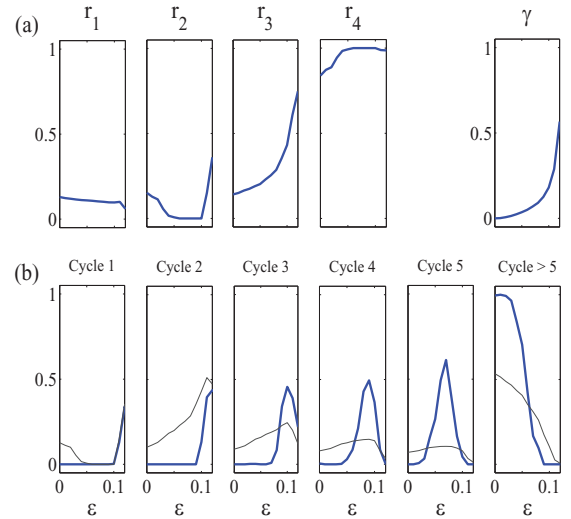


FIG. 9. (Color online) Ring intermittency in coupled Rössler oscillators with parameters  $\varepsilon_1 = 0$ ,  $\varepsilon_2 = \varepsilon$ , and control parameters  $\omega_1 = 1.0$ ,  $\omega_2 = 0.95$ . The ring intermittency occurs between  $\varepsilon_t = 0.1097$  and  $\varepsilon_c = 0.124$ . (a) Rates  $r_i$  and synchronization index  $\gamma$ . (b) Relative frequencies of desynchronization events of different durations. The thick solid line stands for actual duration, while the thin solid line represents the estimates from the transition rates.

## B. Eyelet intermittency

As the coupling strength increases further from the first critical value  $\varepsilon_t$ , exponentially rare  $2\pi$  phase jumps for coupled Rössler oscillators and irregular  $\pm 2\pi$  phase jumps for coupled Lorenz oscillators can be observed before the second critical value  $\varepsilon_c$  where the phase synchronization is established. Since the phase slips are rare, the scaling rule and probability distributions are different from those of the type-I intermittency. Lee *et al.* [8] found the second critical values  $\varepsilon_c = 0.0286$  for coupled Rössler oscillators and  $\varepsilon_c = 12$  for coupled Lorenz oscillators. Note that other parameter values  $\omega_{1,2}$  and  $\gamma_{1,2}$  are the same as in the type-I intermittency. For  $\varepsilon_t < \varepsilon < \varepsilon_c$ , the mean laminar phase length  $\langle \ell \rangle$  obeys the scaling rule

$$\ln(\langle \ell \rangle) \sim -(\varepsilon_c - \varepsilon)^{1/2}. \quad (12)$$

The scaling rule and the corresponding probability distribution of the laminar phase length suggest both systems are in the eyelet intermittency. Since the eyelet intermittency features the longer laminar phase than that of the type-I intermittency,  $r_1$  is smaller than that of the type-I intermittency.

Note that when  $\varepsilon > \varepsilon_c$ , the system is in the first region of the first-return map for phases, that is, in the synchronous region, and the rates  $r_{2,3,4}$  are undefined while the rate  $r_1 = 0$ . However, the phase difference may fluctuate in some smaller limits and synchronization index  $\gamma$  may still be below 1.

Figures 6(a) and 7(a) show that the transition rates  $r_i$  of both coupled Rössler oscillators and coupled Lorenz oscillators are characteristically distinct from one another near and away from the second critical value  $\varepsilon_c$ . In fact, the rate  $r_3$  for coupled Rössler oscillators is substantially smaller than that of coupled Lorenz oscillators for all ranges of  $\varepsilon$ . This small value of  $r_3$  together with the small value of  $r_2 \in (0.25, 0.4)$  for

coupled Rössler oscillators implies that these two oscillators spend a substantially longer time in the desynchronous state once the trajectory leaves the synchronous state than the coupled Lorenz oscillators do. The rates  $r_{2,3,4}$  for coupled Lorenz oscillators show substantial variability while those for the coupled Rössler oscillators do not. Therefore the temporal structure of synchronized and desynchronized events is different in bidirectionally coupled Rössler oscillators and Lorenz oscillators even though the overall synchrony can be similar.

Now let us also consider unidirectionally coupled Rössler oscillators for the eyelet intermittency. We use Eq. (7) with  $\varepsilon_1 = 0$  and  $\varepsilon_2 = \varepsilon$ . When control parameters  $\omega_1 = 0.93$  and  $\omega_2 = 0.95$ , Hramov *et al.* [12] found two critical values  $\varepsilon_t = 0.0345$  and  $\varepsilon_c = 0.042$ . They showed that when  $\varepsilon \in (\varepsilon_t, \varepsilon_c)$ , the intermittent behavior of unidirectionally coupled Rössler oscillators can be classified as the eyelet intermittency. Note that this intermittent behavior can be also treated as the type-I intermittency with noise [12].

During the eyelet intermittency, rate  $r_3$  in Fig. 8(a) experiences substantial variation while that in Fig. 6(a) keeps almost the same level. Rate  $r_4$  in Fig. 8(a) also shows relatively large variation while that in Fig. 6(a) does not. Note that rates  $r_1$  for both systems are almost the same. The large variations also can be observed in the durations of desynchronization events for several cycle lengths (1, 2, > 5) in Fig. 8(b) while almost no variation in Fig. 6(b) is observed. Therefore, their temporal structures of synchronized and desynchronized events are different even though the overall synchrony can be similar.

### C. Ring intermittency

For the ring intermittency, we consider unidirectionally coupled Rössler oscillators. As in Ref. [9], we use Eq. (7) with  $\varepsilon_1 = 0$ ,  $\varepsilon_2 = \varepsilon$ , and control parameters  $\omega_1 = 1.0$ ,  $\omega_2 = 0.95$ . The frequency mismatch between two oscillators is larger than those of the type-I and the eyelet intermittencies discussed in the previous sections. To explore the synchronization behavior more clearly, Hramov *et al.* [9] used the transformation of coordinates,  $\hat{x} = x_2 \cos(\phi_1) + y_2 \sin(\phi_1)$  and  $\hat{y} = -x_2 \sin(\phi_1) + y_2 \cos(\phi_1)$  and plotted the limit cycle in the  $(\hat{x}, \hat{y})$  plane. Then the trajectory on this transformed plane looks like a ring.

Below the boundary of the phase synchronization regime (when  $\varepsilon < \varepsilon_c$ ), the dynamics of the phase difference  $\theta(t)$  is persistently and intermittently interrupted by sudden phase slips ( $2\pi$  jumps). As  $\varepsilon$  increases further, the limit cycle starts to enclose the origin near the first critical point and the phase destruction begins. Two critical values  $\varepsilon_t = 0.1097$  and  $\varepsilon_c = 0.124$  were observed [9] such that (i) the phase synchronization occurs for  $\varepsilon > \varepsilon_c$ , (ii) the (ring) intermittent behavior occurs for  $\varepsilon_t < \varepsilon < \varepsilon_c$ , and (iii) the asynchronous dynamic occurs for  $\varepsilon < \varepsilon_t$ .

Figure 9(a) shows that during the ring intermittency, the rate  $r_1$  slowly decreases. However, the rates  $r_{2,3}$  change drastically during the ring intermittency while  $r_4$  is an almost constant during this parameter regime. These changes of the rates imply that the probabilities of long cycles are getting smaller as the coupling strength increases [see Fig. 9(b)]. On the other hand,

the probabilities of short desynchronizations (lasting for one or two cycles of oscillations) are getting higher.

Now let us compare the ring intermittency in Fig. 9 with the eyelet intermittency in Fig. 8. Both systems are unidirectionally coupled Rössler oscillators, but with different control parameters  $\omega_{1,2}$ .

Since the phase slips in the eyelet intermittency are rare, as one can expect, rate  $r_1$  in Fig. 8(a) has a much smaller value than that in Fig. 9(a). Rate  $r_4$  in Fig. 8(a) has a slightly lower value than that in Fig. 9(a). Rate  $r_2$  in Fig. 9(a) shows a huge fluctuation while that in Fig. 8(a) does not. The probability of long desynchronization events (Cycle > 5) for the ring intermittency is close to zero while that in the eyelet intermittency starts to decrease from a high level (>0.5). Thus, long desynchronization events are dominant for the eyelet intermittency while short desynchronization events are dominant for the ring intermittency.

## V. COUPLED NEURONS EXAMPLE

Intermittency and intermittent and otherwise imperfect synchronization can be observed in the brain in different conditions (for example, see Refs. [17,18,22,23]). Thus it will be useful to apply the method to more realistic neural-like model systems to study what rates  $r_i$  may reveal about synchronized dynamics. We consider two mutually coupled neurons described by a single-compartment conductance-based Hodgkin-Huxley-type equations. We couple these neurons through inhibitory synapses. The details for this kind of a model can be found in, for example, Ref. [24]. The equations for each cell can be written as

$$C_m v' = -I_L - I_{Na} - I_K - I_{syn} + W + I_0, \quad (13)$$

$$x' = \varphi[\alpha_x(v)(1-x) - \beta_x(v)x],$$

where  $I_L = g_L(v - E_L)$ ,  $I_{Na} = g_{Na}m^3(v)h(v - E_{Na})$ ,  $I_K = g_Kn^4(v - E_K)$  represent leak, sodium, and potassium currents, respectively. Independent Gaussian white noise  $W$  with zero mean and a standard deviation of 2.12 is added to both neurons.  $I_0$  is an external current.  $x$  stands for three different gating variables  $m, n$ , and  $h$  with the following  $\alpha(v)$  and  $\beta(v)$ :

$$\begin{aligned} \alpha_n(v) &= 0.01(v + 55)/\{1 - \exp[-(v + 55)/10]\}, \\ \beta_n(v) &= 0.125 \exp[-(v + 65)/80], \\ \alpha_m(v) &= 0.1(v + 40)/\{1 - \exp[-(v + 40)/10]\}, \\ \beta_m(v) &= 4 \exp[-(v + 65)/18], \\ \alpha_h(v) &= 0.07 \exp[-(v + 65)/20], \\ \beta_h(v) &= 1/\{1 + \exp[-(v + 35)/10]\}. \end{aligned} \quad (14)$$

The term  $I_{syn}$  represents the synaptic current. For a cell  $i \in \{1, 2\}$ , the synaptic current  $I_{syn,i} = g_{syn,i}(v_i - v_{syn})s_j$  where  $j \in \{1, 2\} \setminus \{i\}$ . The synaptic variable  $s$  (the fraction of activated synaptic channels) is modeled by the first-order kinetic equation in the form

$$s' = \alpha(1-s)H_\infty(v - \theta_v) - \beta s, \quad (15)$$

where  $H_\infty(x) = 1/(1 + \exp[-x/\sigma_s])$  is a sigmoidal function. The parameter values are the following:  $C_m = 1$ ,  $g_{Na} = 120$ ,  $E_{Na} = 50$ ,  $g_K = 36$ ,  $E_K = -77$ ,  $g_L = 0.3$ ,  $E_L = -54.4$ ,

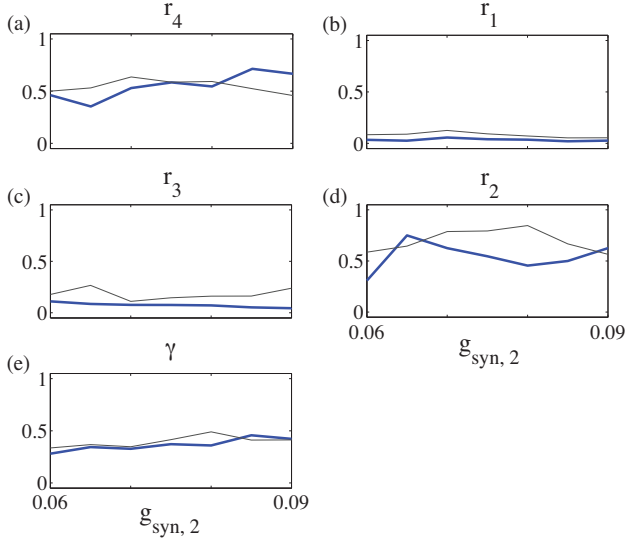


FIG. 10. (Color online) Rates  $r_i$  and synchronization index  $\gamma$  for varied  $g_{\text{syn},2}$  with fixed  $g_{\text{syn},1} = 0.1$ . Although the levels of the synchronization index  $\gamma$  are similar, the rates  $r_2$  and  $r_4$  experience more substantial variation depending on the synaptic strength  $g_{\text{syn},2}$ . Small noise also exerts some influence on the rates, which is not as prominent in  $\gamma$ . The thick solid line is the noiseless case and the thin solid line is for the noise  $W$ .

$v_{\text{syn}} = -85$ ,  $I_0 = 10$ ,  $\varphi = 0.35$ ,  $\theta_v = 0$ ,  $\sigma_s = 5$ ,  $\alpha = 2$ , and  $\beta = 0.05$ . Both cells are self-oscillators in the absence of coupling ( $g_{\text{syn},i} = 0$ ). Voltages  $v$  for both neurons exhibit spiky time series (sequence of action potentials) and were filtered to the gamma-band (30–80 Hz). The Hilbert transform was used to define the phases and then first-return maps were constructed.

Figure 10 shows that the synchronization index  $\gamma$  changes slowly for a range of values of  $g_{\text{syn},2}$  (for fixed  $g_{\text{syn},1} = 0.1$ ), but the rates  $r_i$  exhibit more substantial variations depending on  $g_{\text{syn},2}$ . As can be seen from Figs. 10(a) and 10(d), the rates  $r_{2,4}$  are changing substantially with the similar  $\gamma$ . This implies that the rates describe the fine temporal structure of synchronization and desynchronization events. The rates (and thus the fine temporal structure of synchronous and desynchronous dynamics) may be more affected by noise than synchronization index  $\gamma$  (Fig. 10). Especially for small values of coupling  $g_{\text{syn},2}$  overall degree of phase locking is not influenced by small noise. However, the rates  $r_{2,3,4}$  experience substantial variations and thus the corresponding timing of synchronization and desynchronization events is dependent on the noise level. Therefore, exploring the fine temporal structures of coupled oscillators in experimental data may provide some help in constraining multiple alternatives in modeling studies, like in Ref. [19].

## VI. DISCUSSION

We studied the first-return maps of the phase difference between two oscillatory signals. If there is some phase locking is present on the average, we can study the phase-locking relationship on each cycle of oscillations. The phase space of this map is partitioned into four regions and the transition

rates  $r_i$  between regions are computed. These transition rates characterize the details of temporal dynamics, which are missed by standard synchronization measures [such as  $\gamma$  in Eq. (1)].

Using a series of characteristic model systems, such as coupled skew tent maps (for which the values of Lyapunov exponents can be computed analytically), coupled Rössler and Lorenz oscillators, and coupled Hodgkin-Huxley neuronal models, we showed that the aforementioned transition rates provide a complimentary description of synchronized dynamics. They describe the dynamics away from the synchronized state, so that even if the stability (transversal Lyapunov exponent) of the synchronization manifold and time-series-based measure of synchrony (such as a phase-locking index) are the same, the rates will capture the details of desynchronization events. In an extreme case, the same level of synchrony may be reached with a relatively rare but long desynchronization events and numerous short desynchronization events. The rates allow for discrimination of this alternative.

The duration of desynchronization events can be computed from this approach and is related to the rates (although not necessarily defined by them completely). The traditional analysis of intermittent behavior, including intermittency near synchronization onset, considers duration of laminar (i.e., synchronized in the case of synchronization) episodes. These distributions are universal and depend on the type of intermittency. But the same intermittency type in different systems can naturally have different dynamics of synchronization and desynchronization events (as the reinjection mechanism is not defined by the type of intermittency). We showed how the rates are able to capture this difference and the corresponding difference in the timing of synchronized and desynchronized dynamics.

From the phase-space-based approach point of view, the system spends a substantial fraction of time away from the synchronization manifold in other parts of the phase space. Therefore the stability of this manifold and the bifurcations that it can experience provide incomplete information about the dynamics. The introduced rates  $r_i$  can help to fill this gap. In the time-series-based approach, the global synchronization measures are not designed to describe the relationship between phases on each cycle of oscillations. The approach considered here allows to inspect the phase locking at each cycle of oscillations (naturally, only if some synchronization level is present overall). Recent experimental and modeling results [18,19] indicate that the fine temporal structure of synchronization is important. Here we used standard test systems to explain how the analysis of this structure works.

The methodology considered here can be applied to any appropriate data with some level of phase locking regardless of the mechanisms of synchronous dynamics. We clarified here what this method yields in terms of characterization of the phase space and in terms of the fine temporal structure of phase locking. However, we think in future studies the method may be used as a tool to study some mechanisms of synchrony or at least distinguish between different mechanisms of synchrony (in particular when parameters of coupling cannot be changed in the experiment).

We would like to conclude the paper with four notes regarding the method. First, we want to reiterate that for

this kind of analysis the signals should be phase locked on average. The synchrony is an essentially noninstantaneous phenomenon. Only if there is a preferred phase-locking angle, we can follow deviations from it on each cycle (and that is yet another reason for the necessity of computations of the global synchronization measures or synchrony measure over a moderate size time window, like in Ref. [16]).

Second, the partitioning of the phase space of the  $\phi_{x,i}$  map into four parts is somewhat arbitrary. It simplifies the computation of rates, as there are only four of them. It also implies that if the phases do not deviate from more than  $\pi/2$ , they are considered in synchrony. This appears to be a reasonable assumption for some systems (for example, a smaller tolerance may be easily destroyed by noise and fluctuations, a larger tolerance is less likely to be acceptable for information transmission in the synchronized system). However, in certain applications a finer partitioning may be necessary. This is apparently possible to implement, although the rates will be harder to interpret. Moreover, the major idea of the considered approach, to study how the phase difference deviates from the preferred phase-locking angle, can be considered not only in a discrete-time framework as we did here, but also can be generalized to continuous time.

Third, the approach developed here is agnostic to the presence or absence of noise in the time series. Noise surely can contribute to the generation of imperfect phase locking and affect the transition rates (as in the example in the previous section). The properties of noise may be reflected in the transition rates and the considered methodology may be a tool to study the effect of noise on synchronous dynamics. This appears to be an important subject for future research.

Fourth, if the system is very close to the synchronization threshold, this analysis may not necessarily be very informative because the system will spend most of the time in the synchronized state. However, as we mentioned in the Introduction, synchronization in living systems may be highly variable. In this case, synchronized events may be relatively rare and/or relatively short (although they may still be significant functionally). Thus the approach considered here (as well as its variations) has the potential to describe functionally important temporal features of synchronization and desynchronization dynamics.

#### ACKNOWLEDGMENTS

This study was supported by NIH Grant No. R01NS067200 (NSF/NIH CRCNS).

- 
- [1] A. Pikovsky, M. Rosenblum, and J. Kurths, *Synchronization, A Universal Concept in Nonlinear Sciences* (Cambridge University Press, Cambridge, England, 2001).
  - [2] S. Boccaletti, J. Kurths, G. Osipov, D. Valladares, and C. Zhou, *Phys. Rep.* **366**, 1 (2002).
  - [3] L. Glass, *Nature (London)* **410**, 277 (2001).
  - [4] A. Engel, P. Fries, and W. Singer, *Nat. Rev. Neurosci.* **2**, 704 (2001).
  - [5] G. Buzsáki and A. Draguhn, *Science* **304**, 1926 (2004).
  - [6] T. Nowotny, R. Huerta, and M. Rabinovich, *Chaos* **18**, 037119 (2008).
  - [7] M. Rabinovich, P. Varona, A. Selverston, and H. Abarbanel, *Rev. Mod. Phys.* **78**, 1213 (2006).
  - [8] K. J. Lee, Y. Kwak, and T. K. Lim, *Phys. Rev. Lett.* **81**, 321 (1998).
  - [9] A. E. Hramov, A. A. Koronovskii, M. K. Kurovskaya, and S. Boccaletti, *Phys. Rev. Lett.* **97**, 114101 (2006).
  - [10] S. Rim, I. Kim, P. Kang, Y.-J. Park, and C.-M. Kim, *Phys. Rev. E* **66**, 015205 (2002).
  - [11] L. Zhao, Y.-C. Lai, and C.-W. Shih, *Phys. Rev. E* **72**, 036212 (2005).
  - [12] A. E. Hramov, A. A. Koronovskii, M. K. Kurovskaya, and O. I. Moskalenko, *Phys. Lett. A* **375**, 1646 (2011).
  - [13] A. E. Hramov, A. A. Koronovskii, and M. K. Kurovskaya, *Phys. Rev. E* **78**, 036212 (2008).
  - [14] A. Schnitzler and J. Gross, *Nat. Rev. Neurosci.* **6**, 285 (2005).
  - [15] P. Uhlhaas and W. Singer, *Neuron* **52**, 155 (2006).
  - [16] J. M. Hurtado, L. L. Rubchinsky, and K. A. Sigvardt, *J. Neurophysiol.* **91**, 1883 (2004).
  - [17] J. Hurtado, L. Rubchinsky, K. Sigvardt, V. Wheelock, and C. Pappas, *J. Neurophysiol.* **93**, 1569 (2005).
  - [18] C. Park, R. M. Worth, and L. L. Rubchinsky, *J. Neurophysiol.* **103**, 2707 (2010).
  - [19] C. Park, R. M. Worth, and L. L. Rubchinsky, *Phys. Rev. E* **83**, 042901 (2011).
  - [20] A. Liebhold, W. Koenig, and O. Bjornstad, *Ann. Rev. Ecology, Evolution and Systematics* **35**, 467 (2004).
  - [21] M. G. Rosenblum, A. S. Pikovsky, and J. Kurths, *Phys. Rev. E* **63**, 058201 (2001).
  - [22] A. E. Hramov, A. A. Koronovskii, I. S. Midzyanovskaya, E. Sitnikova, and C. M. V. Rijn, *Chaos* **16**, 043111 (2006).
  - [23] P. Gong, A. R. Nikolaev, and C. van Leeuwen, *Phys. Rev. E* **76**, 011904 (2007).
  - [24] G. B. Ermentrout and D. H. Terman, *Mathematical Foundations of Neuroscience* (Springer, New York, 2010).